



Super-resolution in time-reversal focusing on a moving source



Josselin Garnier^{a,*}, Mathias Fink^b

^a *Laboratoire de Probabilités et Modèles Aléatoires & Laboratoire Jacques-Louis Lions, Université Paris Diderot, 75205 Paris Cedex 13, France*

^b *Institut Langevin, UMR 7587, ESPCI ParisTech and CNRS, 1 rue Jussieu, 75238 Paris Cedex 05, France*

HIGHLIGHTS

- Analysis of time-reversal refocusing on a moving source.
- Quantification of super-resolution effects.
- Comparison of subsonic and supersonic regimes.

ARTICLE INFO

Article history:

Received 30 March 2014

Received in revised form 10 November 2014

Accepted 11 November 2014

Available online 20 November 2014

Keywords:

Time reversal

Super-resolution

Moving sources

ABSTRACT

This paper presents a detailed analysis of time-reversal experiments involving a moving point source that emits a pulse. Different configurations are addressed with full-aperture or partial-aperture time-reversal mirrors and with subsonic or supersonic sources. Doppler effects and lack of source-receiver reciprocity significantly affect the time-reversal refocusing when the velocity of the source becomes comparable as or larger than the speed of propagation. The main result is that refocusing can be enhanced when the velocity of the source becomes close to the speed of propagation compared to the classical diffraction-limited refocusing properties when the source does not move, and this super-resolution effect can be quantified by simple and explicit formulas.

© 2014 Elsevier B.V. All rights reserved.

1. Introduction

Time reversal of waves was extensively studied in the last twenty years (see [1–3] and also [4–6]). A time-reversal mirror consists in a set of transducers that can be used as receivers or as transmitters. A classical time-reversal experiment consists in two steps. In the first step, a source generates a wave that propagates through a medium and is recorded by the time-reversal mirror used as a set of receivers. In the second step, the time-reversal mirror is used as an array of transmitters, it re-emits the time-reversed recorded signals. It turns out that the wave focuses back at the initial source position, as if the wave were being played backwards. The refocusing properties have been studied experimentally, numerically, and theoretically. They are characterized by diffraction-limited focal spots, that is to say, the size of the time-reversed focal spot when the original source is point-like is of the order of the source carrier wavelength. In more detail, when the time-reversal mirror has full aperture, i.e. it completely surrounds the original source, the focal spot has the form of the imaginary part of Green's function, which is a sinc function with a width equal to half-a-wavelength when the medium is homogeneous and three-dimensional [7]. When the time-reversal mirror has finite size, then the size of the focal spot is given by the Rayleigh resolution formula that depends on the numerical aperture of the mirror [8,9].

* Corresponding author.

E-mail addresses: garnier@math.univ-paris-diderot.fr (J. Garnier), mathias.fink@espci.fr (M. Fink).

Enhanced refocusing is a remarkable property observed in many time-reversal experiments. Let us consider the case of a full-aperture time-reversal mirror. The focal spot is expected to be diffraction-limited, with a focal spot diameter equal to the carrier wavelength. Several mechanisms can be responsible for an enhanced refocusing of the time-reversed wave. First, the diffraction limit can be overcome if the source is replaced by its time-reversed image during the second step of the time-reversal experiment. This requires to use an active sink that absorbs the time-reversed wave precisely at the original source location and at the exact refocusing time [10]. Second it is possible to obtain subwavelength focusing when the initial source is in the near field of the time-reversal mirror and the propagating medium is homogeneous [11]. Third, focusing beyond the diffraction limit with far-field time reversal is possible, provided a random distribution of scatterers is placed in the near field of the original source, which locally reduces the effective wavelength [12]. Finally, if we consider limited-aperture time-reversal mirrors, then it is possible to exploit the scattering properties of the background medium to beat the Rayleigh resolution formula. Indeed multiple scattering due to random inhomogeneities in the medium can increase the directional diversity of waves which enhances the time reversal refocusing [13–21].

In this paper we present a new mechanism that can produce enhanced refocusing, for full-aperture time-reversal mirrors, in which case the focal spot will be smaller than the diffraction limit, and for partial-aperture time-reversal mirrors, in which case the focal spot will be smaller than the Rayleigh resolution formula. Indeed we revisit the time-reversal resolution analysis when the original source is moving. Very few results are available when the source is moving. Historically the related problem of the impact of changes in the medium was addressed in [22–24] where it is shown that time-reversal refocusing is degraded by changes in the medium that occur between the two steps of the time-reversal experiment (i.e., between the time that the signal is emitted from its source and the time that the time-reversal array reemits the time-reversed recorded signals). In [25–29,34] the motion of the time-reversal mirror or the one of the source are shown to have little influence for active sonar and underwater communication applications for small velocities. In [30] the impact of small displacements of the target on the invariants of the time-reversal operator is investigated theoretically and experimentally. These studies show that it is possible to quantitatively address time reversal with moving sources and sensors, although the main result that we present in this paper is not exhibited.

In this paper we address both the cases of a full-aperture time-reversal mirror and of a finite-aperture time-reversal mirror. Our main results predict that, when the velocity becomes non-negligible compared to the speed of propagation, then the focal spot size can become smaller than the diffraction limit for full-aperture time-reversal mirrors and than the Rayleigh resolution formula for partial-aperture time-reversal mirrors. These surprising super-resolution effects can be explained from the physical point of view by the Doppler effect, which means that the receivers at the time-reversal mirror record higher frequency components than the original carrier frequency of the source. From the mathematical point of view we show the result in the case of a homogeneous medium by using some integral identities.

The paper is organized as follows. In Section 2 we address the case of a moving source and a full-aperture time-reversal mirror in a three-dimensional homogeneous and open medium. We determine the form of the refocused time-reversed wave and identify the resolution enhancement factors in the transverse and longitudinal directions. In Section 3 we address the case of a partial-aperture time-reversal mirror in a three-dimensional homogeneous and open medium. We show that resolution depends not only on the norm but also on the direction of the velocity vector of the source. In Section 4 we revisit the results in the two-dimensional setting and show that they are similar as those in the three-dimensional set-up.

2. Time reversal with a full-aperture mirror

We consider a point-like source moving in a three-dimensional open medium and emitting a signal with carrier frequency ω_0 and (real-valued) pulse profile $f(t)$. The source position is

$$\vec{\mathbf{X}}(t) = \vec{\mathbf{X}}_0 + vt\vec{\mathbf{e}}_z,$$

where $\vec{\mathbf{e}}_z$ is the unit vector pointing in the z -direction, v the velocity of the source (with $v \geq 0$), and $\vec{\mathbf{X}}_0$ is the position of the source at time 0. We carry out a time-reversal experiment from the signals recorded at the surface of a ball with radius L and center $\mathbf{0}$ and observe the time-reversed field around the original source location. We will see that time reversal with Neumann data leads to super-resolution effects, both in space and time. We first present an integral representation of the time-reversed field in Section 2.1 and then carry out explicit calculations in Sections 2.2 and 2.3 to address subsonic and supersonic sources, respectively, when the source bandwidth is small. Finally, in Section 2.4 we present another approach based on Helmholtz–Kirchhoff identity that allows us to give results valid for arbitrary bandwidth.

2.1. Integral representation of the time-reversed field

In the Fourier domain, the wave field $\hat{u}(\omega, \vec{\mathbf{x}})$ emitted by the source satisfies the Helmholtz equation

$$\Delta \hat{u} + \frac{\omega^2}{c_0^2} \hat{u} = -\hat{s}(\omega, \vec{\mathbf{x}}),$$

where the source term is in the time domain

$$s(t, \vec{\mathbf{x}}) = \delta(\vec{\mathbf{x}} - \vec{\mathbf{X}}(t))e^{-i\omega_0 t}f(t) + c.c.,$$

where *c.c.* stands for complex conjugate (i.e. $s(t) + c.c. = s(t) + \overline{s(t)}$), and in the Fourier domain

$$\hat{s}(\omega, \vec{\mathbf{x}}) := \int_{-\infty}^{\infty} s(t, \vec{\mathbf{x}}) e^{i\omega t} dt = \delta(\mathbf{x} - \mathbf{X}_0) \frac{1}{v} \exp\left(i(\omega - \omega_0) \frac{z - Z_0}{v}\right) f\left(\frac{z - Z_0}{v}\right) + s.c., \quad (1)$$

where *s.c.* means symmetric complex conjugate (i.e. $\hat{s}(\omega) + s.c. = \hat{s}(\omega) + \overline{\hat{s}(-\omega)}$), with the notation $\vec{\mathbf{x}} = (\mathbf{x}, z) \in \mathbb{R}^2 \times \mathbb{R}$ and $\vec{\mathbf{X}}_0 = (\mathbf{X}_0, Z_0)$. Using the three-dimensional homogeneous Green's function,

$$\hat{G}(\omega, \vec{\mathbf{x}}, \vec{\mathbf{x}}') = \frac{1}{4\pi |\vec{\mathbf{x}} - \vec{\mathbf{x}}'|} e^{i\frac{\omega}{c_0} |\vec{\mathbf{x}} - \vec{\mathbf{x}}'|}, \quad (2)$$

the wave field is

$$\hat{u}(\omega, \vec{\mathbf{x}}) = \int_{\mathbb{R}^3} \hat{G}(\omega, \vec{\mathbf{x}}, \vec{\mathbf{x}}') \hat{s}(\omega, \vec{\mathbf{x}}') d\vec{\mathbf{x}}' + s.c.$$

The signals are recorded on the surface of the ball $B(\mathbf{0}, L)$ centered at $\mathbf{0}$ and with radius L , so that the Neumann data set is (in the frequency domain)

$$\left\{ \partial_\nu \hat{u}(\omega, \vec{\mathbf{x}}) + s.c., \vec{\mathbf{x}} \in \partial B(\mathbf{0}, L) \right\}. \quad (3)$$

By emitting the time-reversed data set from the surface of the ball $B(\mathbf{0}, L)$, we obtain the time-reversed wave field:

$$\hat{u}_{\text{tr}}(\omega, \vec{\mathbf{x}}) = \int_{\partial B(\mathbf{0}, L)} \hat{G}(\omega, \vec{\mathbf{x}}, \vec{\mathbf{x}}') \overline{\partial_\nu \hat{u}(\omega, \vec{\mathbf{x}}')} d\sigma(\vec{\mathbf{x}}') + s.c. \quad (4)$$

The refocusing properties of the time-reversed wave field are analyzed below, first for a subsonic source, and then for a supersonic source. In both cases the goal is to show that we can get refocusing with super-resolution, in the sense that the time-reversed wave refocuses with a focal spot that is smaller than the diffraction limit.

2.2. Subsonic source

In this subsection we assume that the velocity v of the source is smaller than the wave velocity c_0 :

$$M := \frac{v}{c_0} \in (0, 1),$$

and we compute the form of the time-reversed wavefield.

If the initial source location $\vec{\mathbf{X}}_0$ is close to the center $\mathbf{0}$, that is to say, $|\vec{\mathbf{X}}_0| \ll L$ and $\frac{\omega_0}{c_0} |\vec{\mathbf{X}}_0|^2 \ll L$, and if the duration T of the function f is small enough so that the source has moved little compared to L during the emission, more exactly, if $vT \ll L$ and $\frac{\omega_0}{c_0} (vT)^2 \ll L$, then the signals recorded at the surface of the ball $B(\mathbf{0}, L)$ have the form

$$\partial_\nu \hat{u}(\omega, \vec{\mathbf{x}}) = \frac{i\omega}{c_0} \frac{1}{4\pi L} \exp\left(i\frac{\omega}{c_0} \left(L - \frac{\vec{\mathbf{X}}_0 \cdot \vec{\mathbf{x}}}{L}\right)\right) \hat{f}\left(\omega \left(1 - M \frac{z}{L}\right) - \omega_0\right) + s.c., \quad |\vec{\mathbf{x}}| = L.$$

The Doppler effect is noticeable. Indeed, if we think of \hat{f} as a Dirac distribution (this is the limit case $f \equiv 1$), then the central frequency recorded at position $\vec{\mathbf{x}} = (\mathbf{x}, z)$ is $\omega_0 / (1 - Mz/L) \in [\omega_0 / (1 + M), \omega_0 / (1 - M)]$.

The recorded signals are time-reversed and reemitted. In the Fourier domain, the time-reversed wave field is (4). If the search point $\vec{\mathbf{x}}$ is close to the center $\mathbf{0}$, that is to say, $|\vec{\mathbf{x}}| \ll L$ and $\frac{\omega_0}{c_0} |\vec{\mathbf{x}}|^2 \ll L$, then the time-reversed wave field is

$$u_{\text{tr}}(t, \vec{\mathbf{x}}) = \frac{-i}{16\pi^2 c_0} \int_{-\infty}^{\infty} d\omega \overline{\hat{f}(\omega - \omega_0)} \int_{-1}^1 dq J_0\left(\frac{\sqrt{1 - q^2} |\omega| |\mathbf{x} - \mathbf{X}_0|}{1 - Mq} \frac{1}{c_0}\right) \exp\left(-i\omega \frac{t + \frac{z - Z_0}{c_0} q}{1 - Mq}\right) \frac{1}{(1 - Mq)^2} + c.c., \quad (5)$$

where J_0 is the Bessel function of the first kind and of zero order.

Main results. In terms of the Mach number $M = v/c_0$, after some calculations (see Appendix A), we find that, when the bandwidth B (of f) is smaller than the carrier frequency ω_0 (in practice $B \leq 0.1\omega_0$ is enough), the refocused wave has the form:

$$u_{\text{tr}}(t, \vec{\mathbf{x}}) = \frac{-i\omega_0}{4\pi c_0 (1 - M^2)} \text{sinc}\left(\frac{\omega_0}{c_0} \sqrt{\frac{|\mathbf{x} - \mathbf{X}_0|^2}{1 - M^2} + \frac{(z - Z_0 + Mc_0 t)^2}{(1 - M^2)^2}}\right) \times \exp\left(-i\omega_0 \frac{t + M \frac{z - Z_0}{c_0}}{1 - M^2}\right) f\left(-\frac{t + M \frac{z - Z_0}{c_0}}{1 - M^2}\right) + c.c., \quad (6)$$

where $\text{sinc}(q) = \sin(q)/q$. The sinc function is also known as the spherical Bessel function of the first kind and of zero order j_0 . The modulus of the refocused wave profile is plotted in Fig. 1 at time $t = 0$ for $f \equiv 1$.

In the limit case $M = 0$ we recover the standard isotropic sinc function for the refocused spatial profile with a diameter equal to the carrier wavelength, and we recover the time-reversed initial pulse profile.

When $M \in (0, 1)$ the classical time-reversed refocused spatial profile undergoes several modifications:

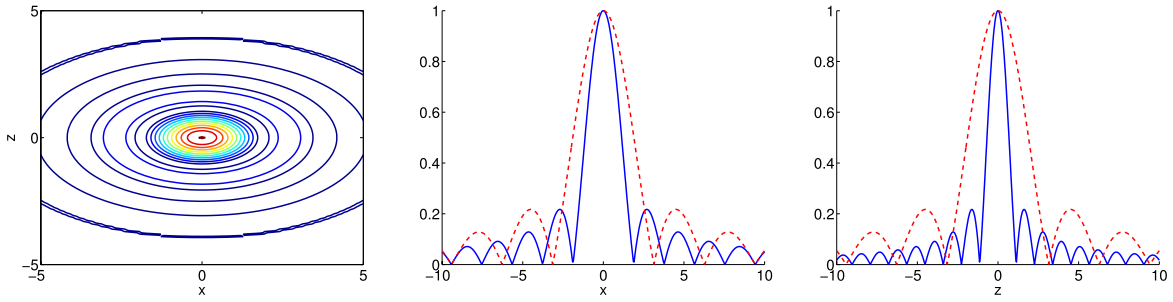


Fig. 1. Spatial profile of the time-reversed refocused wave at $t = 0$ with Neumann data when $M = v/c_0 = 0.8$. In the center and right figures, the dashed red lines are the standard sinc function when the source does not move. The profiles are normalized so that their maximum is one. (For interpretation of the references to color in this figure legend, the reader is referred to the web version of this article.)

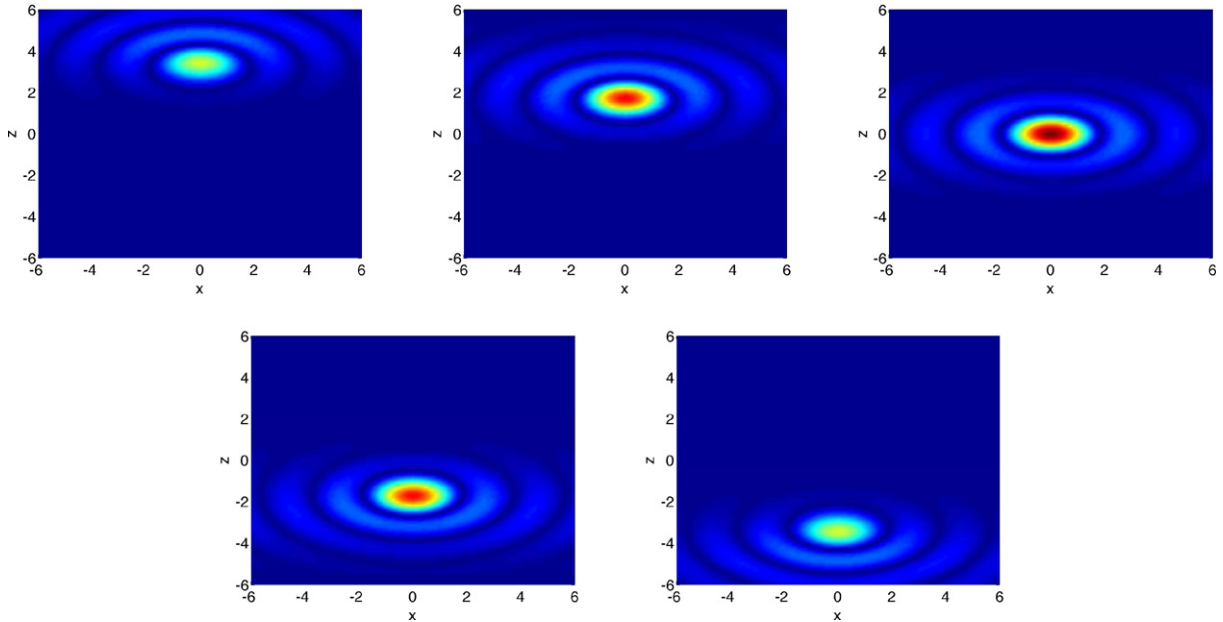


Fig. 2. Spatial profile of the time-reversed refocused wave at $t = -4$ (top left), $t = -2$ (top center), $t = 0$ (top right), $t = 2$ (bottom left), $t = 4$ (bottom right) with Neumann data when $M = v/c_0 = 0.8$, $\omega_0 = 1$, $c_0 = 1$, and the source pulse is $f(t) = \exp(-B^2 t^2)$, $B = 0.1$.

- First, the carrier frequency is increased to the value $\omega_0/(1 - M^2)$. Note that it is the arithmetic average of the carrier frequencies recorded by the mirror which belong to the interval $[\omega_0/(1 + M), \omega_0/(1 - M)]$.
- Second, the center of the refocused wave profile follows the time-reversed trajectory of the original source (see Fig. 2).
- Third, spatial refocusing is enhanced when the source is moving, both in the longitudinal direction of the source motion and in the transverse directions. The enhancement factor is larger in the longitudinal direction than in the transverse ones ($1/(1 - M^2)$ versus $1/\sqrt{1 - M^2}$). This enhancement can be related to the Doppler effect, which means that the recorded signals contain higher frequencies than in the case when the source does not move. Therefore the classical diffraction limit is in fact not violated by this super-resolution phenomenon.

Remark. For the sake of completeness we describe in Appendix B the time-reversed refocused wave obtained with Dirichlet data (i.e. \hat{u} instead of $\partial_\nu \hat{u}$ in (3)–(4)). The results are qualitatively the same ones, although we can notice a quantitatively sharper refocusing for Neumann data (compare Figs. 1 and B.1). That is why we focus our attention on Neumann data in this paper.

2.3. Supersonic source

We consider the same situation as in the previous subsection, but we assume now that the source speed v is larger than the wave velocity c_0 (i.e. $M = v/c_0 > 1$). The expressions of the recorded signals are the same ones as in the subsonic case. This means that there is a singularity in the amplitude of the recorded signals at $\vec{\mathbf{x}} = (\mathbf{x}, L) \in \partial B(\mathbf{0}, L)$ such that $Mz = L$, that is to say points of the form $(|\mathbf{x}|, z) = L(\sqrt{1 - 1/M^2}, 1/M)$.

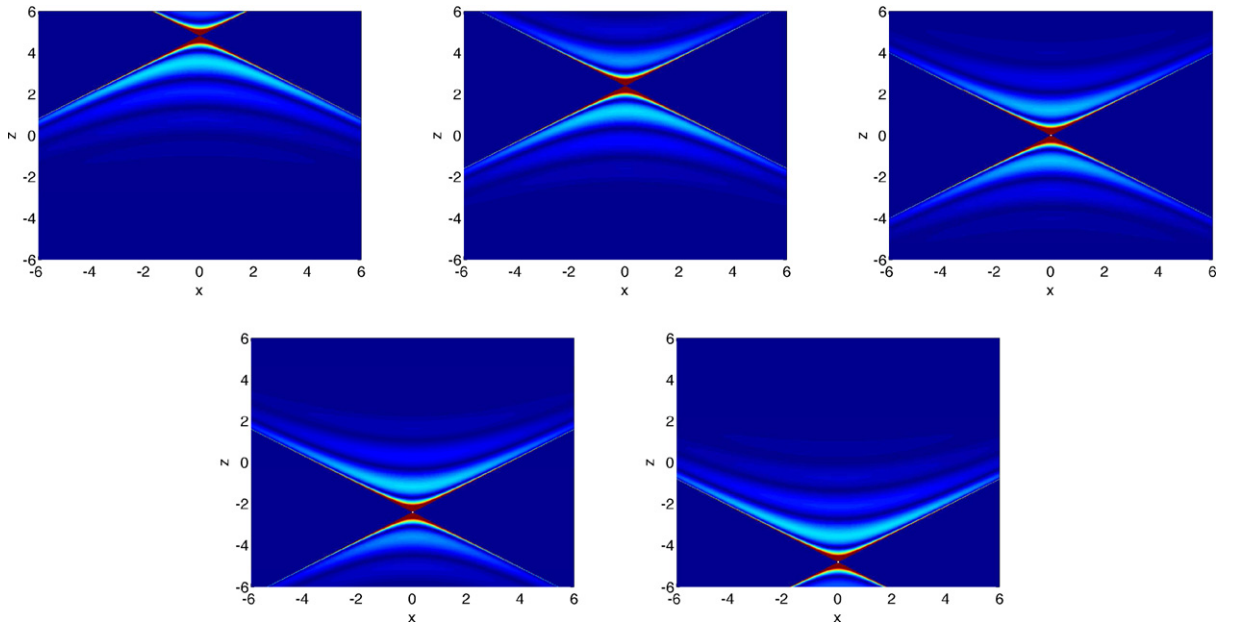


Fig. 3. Spatial profile of the time-reversed refocused wave at $t = -4, -2, 0, 2, 4$ with Neumann data when $M = v/c_0 = 1.2$, $\omega_0 = 1$, $c_0 = 1$, and the source pulse is $f(t) = \exp(-B^2 t^2)$ with $B = 0.1$.

Around the original source location, the refocused wave has the form

$$u_{\text{tr}}(t, \vec{\mathbf{x}}) = \frac{-i}{16\pi^2 c_0} \int_{-\infty}^{\infty} d\omega \overline{\hat{f}(\omega - \omega_0)} \int_{-1}^1 dq j_0 \left(\frac{\sqrt{1-q^2} |\omega| |\mathbf{x} - \mathbf{X}_0|}{c_0} \right) \exp \left(-i\omega \frac{t + \frac{z-Z_0}{c_0} q}{1-Mq} \right) \frac{\text{sgn}(1-Mq)}{(1-Mq)^2} + c.c., \quad (7)$$

where $\text{sgn}(q) = 1$ if $q > 0$, -1 if $q < 0$, and 0 if $q = 0$.

Main results. In terms of the Mach number $M = v/c_0$, after some calculations (see Appendix A), we find that, when the bandwidth (of f) is smaller than the carrier frequency ω_0 , the refocused wave has the form:

$$u_{\text{tr}}(t, \vec{\mathbf{x}}) = \frac{\omega_0 \text{sgn}(z - Z_0 + Mc_0 t)}{4\pi(M^2 - 1)c_0} \Phi \left(\frac{\omega_0 |z - Z_0 + Mc_0 t|}{c_0}, \frac{\omega_0 |\mathbf{x} - \mathbf{X}_0|}{c_0 \sqrt{M^2 - 1}} \right) \times \exp \left(i\omega_0 \frac{t + M \frac{z-Z_0}{c_0}}{M^2 - 1} \right) f \left(\frac{t + M \frac{z-Z_0}{c_0}}{M^2 - 1} \right) + c.c., \quad (8)$$

where

$$\Phi(a, b) = \begin{cases} 0 & \text{if } a < b, \\ y_0(\sqrt{a^2 - b^2}) & \text{if } a > b, \end{cases} \quad (9)$$

and the function $y_0(s) = -\cos(s)/s$ is known as the spherical Bessel function of the second kind and of zero order. We can notice that:

- The carrier frequency is $\omega_0/(M^2 - 1)$.
- Outside the Mach cone, the refocused wave is vanishing. The Mach cone is defined by the usual formula $|z - Z_0 + vt| = \sqrt{M^2 - 1} |\mathbf{x} - \mathbf{X}_0|$.
- The center of the refocused wave profile follows the time-reversed trajectory of the original source $\vec{\mathbf{X}}(-t)$, which can be identified with infinite resolution as it is precisely at the interaction of the two Mach cones $z - Z_0 + vt = \pm \sqrt{M^2 - 1} |\mathbf{x} - \mathbf{X}_0|$ (see Fig. 3). Infinite resolution can be reached here because we assume that the receivers can record all frequencies, and that the sources of the mirror can reemit all frequencies. This is possible if backpropagation is carried out numerically, but this is difficult if a physical time reversal experiment is performed.

2.4. Application of the Helmholtz–Kirchhoff identity

The goal of this subsection is to propose another approach based on integral equations to study time reversal. This approach is less transparent than the direct calculations carried out in the two previous subsections, which allowed to characterize the Doppler effect, but it gives explicit expressions valid for any bandwidth.

We recall that the general expression of the time-reversed field is

$$\hat{u}_{\text{tr}}(\omega, \vec{\mathbf{x}}) = \int_{\mathbb{R}^3} \int_{\partial B(\mathbf{0}, L)} \hat{G}(\omega, \vec{\mathbf{x}}, \vec{\mathbf{x}}') \overline{\partial_\nu \hat{G}(\omega, \vec{\mathbf{x}}', \vec{\mathbf{y}}) \hat{s}(\omega, \vec{\mathbf{y}})} d\sigma(\vec{\mathbf{x}}') d\vec{\mathbf{y}} + s.c.$$

If L is large, the application of the Helmholtz–Kirchhoff identity (see, for instance [31, p. 419] or [32, Theorem 2.33]) gives

$$\hat{u}_{\text{tr}}(\omega, \vec{\mathbf{x}}) = -\frac{1}{2} \int_{\mathbb{R}^3} [\hat{G}(\omega, \vec{\mathbf{x}}, \vec{\mathbf{y}}) - \overline{\hat{G}(\omega, \vec{\mathbf{x}}, \vec{\mathbf{y}})}] \hat{s}(\omega, \vec{\mathbf{y}}) d\vec{\mathbf{y}} + s.c.$$

By substituting the expression of the three-dimensional Green’s function (2) and the one of the moving source (1), we get for $\vec{\mathbf{x}} = (\mathbf{x}, z)$:

$$\hat{u}_{\text{tr}}(\omega, \vec{\mathbf{x}}) = \frac{-i}{4\pi} \int_{-\infty}^{\infty} \frac{\sin\left(\frac{\omega}{c_0} \sqrt{(z - Z_0 - v\tau)^2 + |\mathbf{x} - \mathbf{X}_0|^2}\right)}{\sqrt{(z - Z_0 - v\tau)^2 + |\mathbf{x} - \mathbf{X}_0|^2}} e^{-i(\omega - \omega_0)\tau} f(\tau) d\tau + s.c., \tag{10}$$

in the frequency domain, and

$$u_{\text{tr}}(t, \vec{\mathbf{x}}) = \frac{1}{8\pi} \int_{-\infty}^{\infty} \frac{1}{\sqrt{(z - Z_0 - v\tau)^2 + |\mathbf{x} - \mathbf{X}_0|^2}} \left[\delta(\phi_+(\tau; t, \vec{\mathbf{x}})) - \delta(\phi_-(\tau; t, \vec{\mathbf{x}})) \right] e^{i\omega_0\tau} f(\tau) d\tau + c.c., \tag{11}$$

$$\phi_{\pm}(\tau; t, \vec{\mathbf{x}}) = \tau + t \pm \frac{1}{c_0} \sqrt{(z - Z_0 - v\tau)^2 + |\mathbf{x} - \mathbf{X}_0|^2}, \tag{12}$$

in the time domain. This expression is valid for any velocity of the source. The evaluation of the two Dirac distributions involves the zeros of ϕ_{\pm} and it depends on the subsonic or supersonic character of the source motion. As we see below this analysis gives the same expressions for the time-reversed field as the ones obtained in the previous subsections when the bandwidth is small.

We consider the subsonic case $M = v/c_0 \in (0, 1)$. The equation $\phi_{\pm}(\tau) = 0$ has a unique solution

$$\tau_{\pm} = \frac{-M(z - Z_0) - c_0 t \mp \sqrt{\Delta(t, \vec{\mathbf{x}})}}{c_0(1 - M^2)}, \quad \Delta(t, \vec{\mathbf{x}}) = (z - Z_0 + vt)^2 + (1 - M^2)|\mathbf{x} - \mathbf{X}_0|^2, \tag{13}$$

and we have $\sqrt{(z - Z_0 - v\tau_{\pm})^2 + |\mathbf{x} - \mathbf{X}_0|^2} \phi'_{\pm}(\tau_{\pm}) = \sqrt{\Delta(t, \vec{\mathbf{x}})}$. As a result (11) gives

$$u_{\text{tr}}(t, \vec{\mathbf{x}}) = \frac{1}{8\pi \sqrt{\Delta(t, \vec{\mathbf{x}})}} \left[f(\tau_+) e^{i\omega_0\tau_+} - f(\tau_-) e^{i\omega_0\tau_-} \right] + c.c. \tag{14}$$

This expression is exact whatever the bandwidth of f . If the bandwidth is smaller than the carrier frequency, then the expression can be simplified into

$$u_{\text{tr}}(t, \vec{\mathbf{x}}) = \frac{-i\omega_0}{4\pi c_0(1 - M^2)} \text{sinc}\left(\frac{\omega_0 \sqrt{\Delta(t, \vec{\mathbf{x}})}}{c_0(1 - M^2)}\right) \exp\left(i\omega_0 \frac{-M \frac{z - Z_0}{c_0} - t}{1 - M^2}\right) f\left(\frac{-M \frac{z - Z_0}{c_0} - t}{1 - M^2}\right) + c.c., \tag{15}$$

which is exactly (6).

We consider the supersonic case $M > 1$. Let ϕ_{\pm} be defined by (12). The equation $\phi_{\pm}(\tau) = 0$ has no solution if $|z - Z_0 + vt|^2 < (M^2 - 1)|\mathbf{x} - \mathbf{X}_0|^2$ (because then $\Delta(t, \vec{\mathbf{x}}) < 0$), and as a result (11) gives

$$u_{\text{tr}}(t, \vec{\mathbf{x}}) = 0, \tag{16}$$

in agreement with (8).

Let us now consider a point such that $|z - Z_0 + vt|^2 > (M^2 - 1)|\mathbf{x} - \mathbf{X}_0|^2$. If $z - Z_0 + vt > 0$, then the equation $\phi_+(\tau) = 0$ has no solution while the equation $\phi_-(\tau) = 0$ has two solutions τ_- and τ_+ given by (13). If $z - Z_0 + vt < 0$, then the equation $\phi_-(\tau) = 0$ has no solution while the equation $\phi_+(\tau) = 0$ has two solutions τ_- and τ_+ given by (13). As a result (11) gives

$$u_{\text{tr}}(t, \vec{\mathbf{x}}) = \frac{-\text{sgn}(z - Z_0 + vt)}{8\pi \sqrt{\Delta(t, \vec{\mathbf{x}})}} \left[f(\tau_-) e^{i\omega_0\tau_-} + f(\tau_+) e^{i\omega_0\tau_+} \right] + c.c. \tag{17}$$

This expression is exact whatever the bandwidth of f . If the bandwidth is smaller than the carrier frequency, then the expression can be simplified into

$$u_{\text{tr}}(t, \vec{\mathbf{x}}) = \frac{\omega_0 \text{sgn}(z - Z_0 + vt)}{4\pi c_0(M^2 - 1)} y_0 \left(\frac{\omega_0 \sqrt{\Delta(t, \vec{\mathbf{x}})}}{c_0(M^2 - 1)} \right) \exp\left(i\omega_0 \frac{M \frac{z - Z_0}{c_0} + t}{M^2 - 1}\right) f\left(\frac{M \frac{z - Z_0}{c_0} + t}{M^2 - 1}\right) + c.c., \tag{18}$$

where $y_0(q) = -\cos(q)/q$, which is exactly (8).

3. Time reversal with a partial mirror

In Section 2 we assumed that the time-reversal mirror has full aperture and lies at the surface of the ball $B(\mathbf{0}, L)$. We revisit the results in the case in which the mirror has partial aperture and lies in the square $[-a/2, a/2]^2 \times \{0\}$. The goal is to compute the time-reversed wave field and to exhibit an enhanced refocusing phenomenon, which here means to go beyond the Rayleigh resolution formula.

We consider a moving point-like source emitting a signal with carrier frequency ω_0 and pulse profile $f(t)$. The source position is

$$\vec{\mathbf{X}}(t) = \vec{\mathbf{X}}_0 + \vec{\mathbf{V}}_0 t,$$

where $\vec{\mathbf{X}}_0 = (\mathbf{X}_0, Z_0)$ and $\vec{\mathbf{V}}_0 = (\mathbf{V}_x, V_z)$. We consider the situation in which $|\mathbf{X}_0| \ll Z_0$ and $\lambda_0 \ll a \ll Z_0$. This means that we can expand for any $\vec{\mathbf{x}} = (\mathbf{x}, 0) \in [-a/2, a/2]^2 \times \{0\}$:

$$|\vec{\mathbf{x}} - \vec{\mathbf{X}}(t)| = Z_0 + \frac{|\mathbf{X}_0 - \mathbf{x}|^2}{2Z_0} + V_z t + \mathbf{V}_x t \cdot \frac{\mathbf{X}_0 - \mathbf{x}}{Z_0}.$$

This is the so-called paraxial regime. We also assume that the bandwidth B of the source is smaller than the carrier frequency ω_0 . Therefore, the normal derivative of the field recorded at the time-reversal mirror is

$$\partial_v \hat{u}(\omega, \vec{\mathbf{x}}) = -\frac{i\omega}{4\pi c_0 Z_0} \exp\left(i\frac{\omega}{c_0}\left(Z_0 + \frac{|\mathbf{x} - \mathbf{X}_0|^2}{2Z_0}\right)\right) \hat{f}\left(\omega\left(1 + \frac{V_z}{c_0} + \frac{\mathbf{V}_x \cdot (\mathbf{X}_0 - \mathbf{x})}{c_0 Z_0}\right) - \omega_0\right) + \text{s.c.},$$

for $\vec{\mathbf{x}} = (\mathbf{x}, 0)$, $\mathbf{x} \in [-a/2, a/2]^2$. The time-reversed wave field for $\vec{\mathbf{x}} = \vec{\mathbf{X}}_0 + (\xi, \eta)$ with $|\eta| \ll Z_0$ and $\frac{\omega_0}{c_0} |\xi|^2 \ll Z_0$ is

$$u_{\text{tr}}(t, \vec{\mathbf{x}}) = \frac{1}{(4\pi Z_0)^2 c_0} \int_{[-a/2, a/2]^2} i\omega_0 \exp\left(i\frac{\omega_0}{c_0} \frac{-c_0 t + \eta + \frac{\xi \cdot (\mathbf{X}_0 - \mathbf{x}')}{Z_0} - \frac{\eta |\mathbf{X}_0 - \mathbf{x}'|^2}{2Z_0^2}}{1 + \frac{V_z}{c_0} + \frac{\mathbf{V}_x \cdot (\mathbf{X}_0 - \mathbf{x}')}{c_0 Z_0}}\right) \\ \times \frac{\text{sgn}\left(1 + \frac{V_z}{c_0} + \frac{\mathbf{V}_x \cdot (\mathbf{X}_0 - \mathbf{x}')}{c_0 Z_0}\right)}{\left(1 + \frac{V_z}{c_0} + \frac{\mathbf{V}_x \cdot (\mathbf{X}_0 - \mathbf{x}')}{c_0 Z_0}\right)^2} f\left(\frac{-c_0 t + \eta + \frac{\xi \cdot (\mathbf{X}_0 - \mathbf{x}')}{Z_0} - \frac{\eta |\mathbf{X}_0 - \mathbf{x}'|^2}{2Z_0^2}}{c_0 \left(1 + \frac{V_z}{c_0} + \frac{\mathbf{V}_x \cdot (\mathbf{X}_0 - \mathbf{x}')}{c_0 Z_0}\right)}\right) d\mathbf{x}' + \text{c.c.}$$

This expression can be further simplified but we need to specify two cases depending on the bandwidth.

Main results. If the bandwidth B is such that $a^2/Z_0^2 \ll B/\omega_0 \ll 1$, then the time-reversed wave field in the neighborhood of time $t = 0$ and point (\mathbf{X}_0, Z_0) is of the form

$$u_{\text{tr}}(t, \vec{\mathbf{x}}) = \frac{i\omega_0 a^2 \text{sgn}(1 + M_v)}{(4\pi Z_0)^2 c_0 (1 + M_v)^2} \prod_{j=1}^2 \text{sinc}\left(\frac{\omega_0 a}{2c_0 Z_0 (1 + M_v)^2} \left(\left(\xi_j - \eta \frac{X_{0j}}{Z_0}\right) \left(1 + \frac{V_z}{c_0}\right) - \frac{V_{xj}}{c_0} (\eta - c_0 t)\right)\right) \\ \times \exp\left(i\frac{\omega_0}{c_0 (1 + M_v)} \left(\eta \left(1 - \frac{|\mathbf{X}_0|^2}{2Z_0^2}\right) + \xi \cdot \frac{\mathbf{X}_0}{Z_0} - c_0 t\right)\right) f\left(\frac{\eta \left(1 - \frac{|\mathbf{X}_0|^2}{2Z_0^2}\right) + \xi \cdot \frac{\mathbf{X}_0}{Z_0} - c_0 t}{c_0 (1 + M_v)}\right) + \text{c.c.}, \quad (19)$$

where we have introduced the parameter

$$M_v = \frac{V_z}{c_0} + \frac{\mathbf{V}_x \cdot \mathbf{X}_0}{c_0 Z_0} = \frac{\vec{\mathbf{V}}_0 \cdot \vec{\mathbf{X}}_0}{c_0 Z_0}. \quad (20)$$

The Doppler effect is responsible for a shift in the carrier frequency of the recorded data that becomes $\omega_0/|1 + M_v|$. As a result the cross-range resolution is the standard Rayleigh resolution formula $\lambda_{\text{eff}} Z_0/a$, with $\lambda_{\text{eff}} = \lambda_0 |1 + M_v|$. The range resolution is c_0/B_{eff} , with $B_{\text{eff}} = B/|1 + M_v|$ (see Fig. 4). Note that, contrarily to the full-aperture case, the center of the refocused wave profile does not follow the time-reversed trajectory of the original source. It is a wave profile that comes from the time-reversal array and that propagates at velocity c_0 .

If $B/\omega_0 \ll a^2/Z_0^2 \ll 1$ (quasi-monochromatic case), then

$$u_{\text{tr}}(t, \vec{\mathbf{x}}) = \frac{i\omega_0 a^2 \text{sgn}(1 + M_v)}{(4\pi Z_0)^2 c_0 (1 + M_v)^2} \exp\left(i\frac{\omega_0}{c_0 (1 + M_v)} \left(\eta \left(1 - \frac{|\mathbf{X}_0|^2}{2Z_0^2}\right) + \xi \cdot \frac{\mathbf{X}_0}{Z_0} - c_0 t\right)\right) f(0) \\ \times \prod_{j=1}^2 \Psi\left(\frac{\omega_0 a}{c_0 Z_0 (1 + M_v)^2} \left(\left(\xi_j - \eta \frac{X_{0j}}{Z_0}\right) \left(1 + \frac{V_z}{c_0}\right) - \frac{V_{xj}}{c_0} (\eta - c_0 t)\right), \frac{\omega_0 a^2}{2c_0 Z_0^2 (1 + M_v)} \eta\right) + \text{c.c.}, \quad (21)$$

$$\Psi(\xi, \tilde{\eta}) = \int_{-1/2}^{1/2} \exp(-iq\xi - iq^2\tilde{\eta}) dq. \quad (22)$$

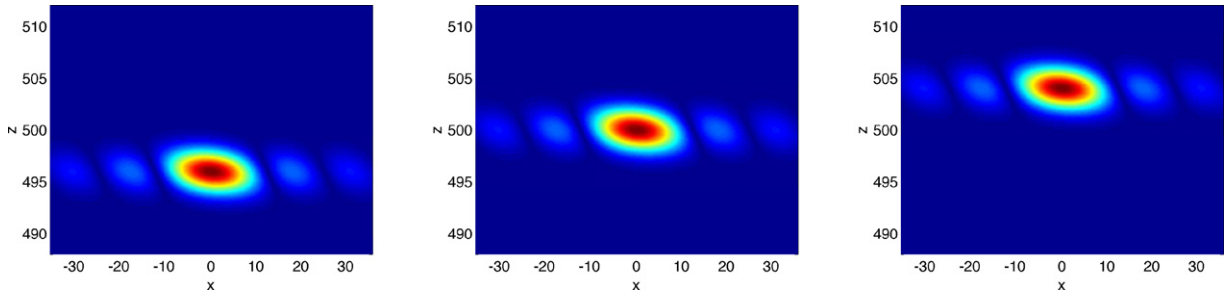


Fig. 4. Spatial profile of the time-reversed refocused wave at $t = 0$ when $V_z = -0.8$, $\mathbf{V}_x = (-0.2, 0)$ for $t = -4$ (left), $t = 0$ (center), and $t = 4$ (right). Here $\omega_0 = 1$, $c_0 = 1$, $a = 50$, $B = 0.1$, $Z_0 = 500$, $\mathbf{X}_0 = \mathbf{0}$, $f(t) = \exp(-B^2 t^2)$.

The marginal formulas can be expressed in terms of tabulated functions:

$$\Psi(\tilde{\xi}, 0) = \text{sinc}\left(\frac{\tilde{\xi}}{2}\right), \quad \Psi(0, \tilde{\eta}) = \frac{2}{\sqrt{|\tilde{\eta}|}}(C - iS)\left(\frac{\sqrt{|\tilde{\eta}|}}{2}\right),$$

where C and S are the Fresnel integrals

$$C(x) = \int_0^x \cos(q^2) dq, \quad S(x) = \int_0^x \sin(q^2) dq.$$

Here the cross-range resolution is $\lambda_{\text{eff}} Z_0 / a$ and the range resolution is $\lambda_{\text{eff}} Z_0^2 / a^2$, with $\lambda_{\text{eff}} = \lambda_0 |1 + M_v|$.

These results demonstrate that the motion of the source affects the resolution of time-reversal refocusing in a three-dimensional open medium with a partial-aperture mirror. The enhancement factor depends on the velocity vector. If the velocity vector of the source is pointed towards the time-reversal array, then $M_v < 0$ and the resolution is enhanced. If the velocity vector is pointed away from the time-reversal array, then $M_v > 0$ and the resolution is reduced. This can be interpreted as a consequence of Doppler effect.

4. Two-dimensional case

4.1. Two-dimensional time reversal with a full-aperture mirror

We revisit the analysis of the time-reversal experiment in a two-dimensional set-up, for a moving source with position $\vec{\mathbf{X}}(t) = \vec{\mathbf{X}}_0 + vt\vec{\mathbf{e}}_z$ (with $v > 0$) and for a time-reversal mirror that covers the surface of the disk $B(\mathbf{0}, L)$ with center $\mathbf{0}$ and radius L . As we will see, the results about time-reversal refocusing are similar as in the three-dimensional set-up, in particular the resolution enhancement factors are the same ones.

The general expression of the time-reversed field is

$$\hat{u}_{\text{tr}}(\omega, \vec{\mathbf{x}}) = \int_{\mathbb{R}^2} \int_{\partial B(\mathbf{0}, L)} \hat{G}(\omega, \vec{\mathbf{x}}, \vec{\mathbf{x}}') \partial_n \overline{\hat{G}(\omega, \vec{\mathbf{x}}', \vec{\mathbf{y}})} \hat{s}(\omega, \vec{\mathbf{y}}) d\sigma(\vec{\mathbf{x}}') d\vec{\mathbf{y}} + s.c.$$

If L is large, the application of the Helmholtz–Kirchhoff identity gives

$$\hat{u}_{\text{tr}}(\omega, \vec{\mathbf{x}}) = -\frac{1}{2} \int_{\mathbb{R}^2} [\hat{G}(\omega, \vec{\mathbf{x}}, \vec{\mathbf{y}}) - \overline{\hat{G}(\omega, \vec{\mathbf{x}}, \vec{\mathbf{y}})}] \hat{s}(\omega, \vec{\mathbf{y}}) d\vec{\mathbf{y}} + s.c.$$

By substituting the expression of the two-dimensional Green’s function:

$$G(t, \vec{\mathbf{x}}, \vec{\mathbf{y}}) = \frac{1}{2\pi} \mathbf{1}_{t - \frac{|\vec{\mathbf{x}} - \vec{\mathbf{y}}|}{c_0} \geq 0} \frac{1}{\sqrt{t^2 - \frac{|\vec{\mathbf{x}} - \vec{\mathbf{y}}|^2}{c_0^2}}},$$

$$\hat{G}(\omega, \vec{\mathbf{x}}, \vec{\mathbf{y}}) = \frac{i}{4} H_0^{(1)}\left(\frac{\omega}{c_0} |\vec{\mathbf{x}} - \vec{\mathbf{y}}|\right),$$

where $H_0^{(1)}$ is a Hankel function, also known as the Bessel function of the third kind and zero order, whose real part is J_0 , and the one of the moving source:

$$s(t, \vec{\mathbf{x}}) = \delta(\vec{\mathbf{x}} - \vec{\mathbf{X}}(t)) e^{-i\omega_0 t} f(t) + c.c.,$$

$$\hat{s}(\omega, \vec{\mathbf{x}}) = \delta(x - X_0) \frac{1}{v} \exp\left(i(\omega - \omega_0) \frac{z - Z_0}{v}\right) f\left(\frac{z - Z_0}{v}\right) + s.c.,$$

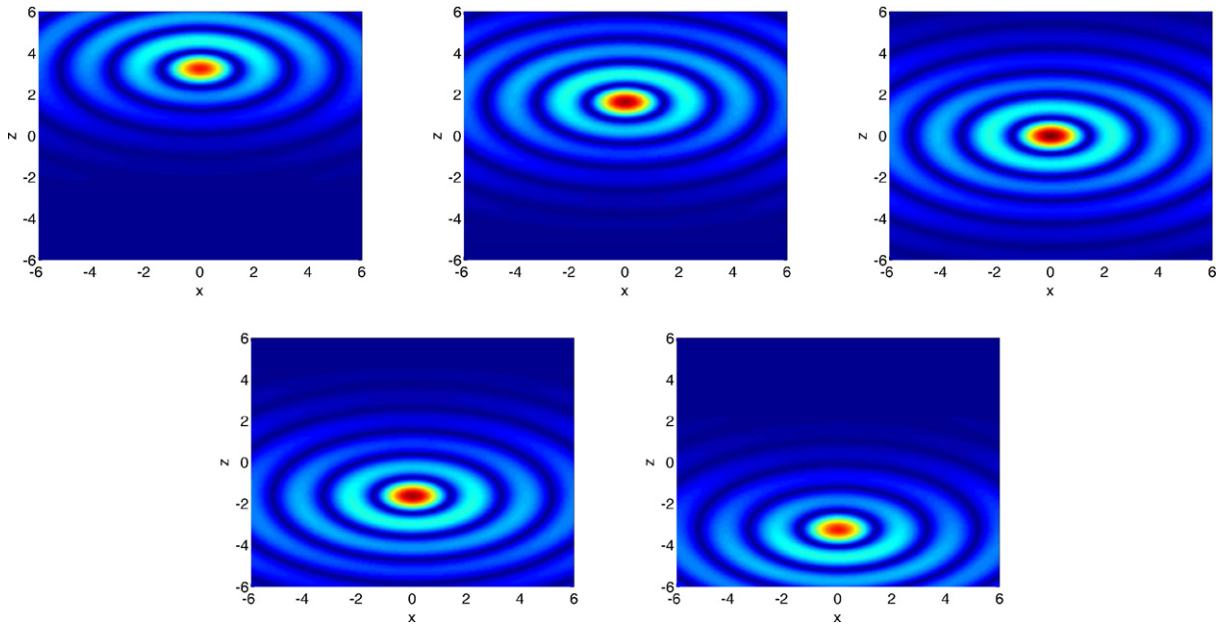


Fig. 5. Spatial profile of the time-reversed refocused wave at $t = -4, -2, 0, 2, 4$ with Neumann data when $M = v/c_0 = 0.8$, $\omega_0 = 1$, $c_0 = 1$, and the source pulse is $f(t) = \exp(-B^2 t^2)$, $B = 0.1$. The set-up is two-dimensional.

we get for $\vec{\mathbf{x}} = (x, z) \in \mathbb{R} \times \mathbb{R}$:

$$u_{\text{tr}}(t, \vec{\mathbf{x}}) = \frac{1}{4\pi} \int_{-\infty}^{\infty} \frac{f(\tau) e^{i\omega_0 \tau}}{\sqrt{(t+\tau)^2 - \frac{|\vec{\mathbf{x}} - \vec{\mathbf{X}}(\tau)|^2}{c_0^2}}} \left(\mathbf{1}_{\frac{|\vec{\mathbf{x}} - \vec{\mathbf{X}}(\tau)|}{c_0} \leq -t-\tau} \mathbf{1}_{\tau+t \leq 0} - \mathbf{1}_{\frac{|\vec{\mathbf{x}} - \vec{\mathbf{X}}(\tau)|}{c_0} \leq t+\tau} \mathbf{1}_{\tau+t \geq 0} \right) d\tau + c.c.,$$

in the time domain, and

$$\hat{u}_{\text{tr}}(\omega, \vec{\mathbf{x}}) = \frac{-i}{4} \int_{-\infty}^{\infty} J_0\left(\frac{\omega}{c_0} |\vec{\mathbf{x}} - \vec{\mathbf{X}}(\tau)|\right) e^{-i(\omega - \omega_0)\tau} f(\tau) d\tau + s.c., \quad (23)$$

in the frequency domain (with the convention $J_0(-q) = -J_0(q)$). These expressions are valid for any velocity of the source. Explicit expressions of the refocused wave profile depends on the velocity of the source (subsonic or supersonic) as explained in [Appendix C](#).

Main results. In the subsonic regime $M := v/c_0 \in (0, 1)$, if the bandwidth of f is smaller than ω_0 , then we find

$$u_{\text{tr}}(t, \vec{\mathbf{x}}) = \frac{-i}{4\sqrt{1-M^2}} \exp\left(-i\omega_0 \frac{t + M \frac{z-Z_0}{c_0}}{1-M^2}\right) f\left(-\frac{t + M \frac{z-Z_0}{c_0}}{1-M^2}\right) J_0\left(\frac{\omega_0}{c_0} \sqrt{\frac{(z-Z_0 + Mc_0 t)^2}{(1-M^2)^2} + \frac{(x-X_0)^2}{1-M^2}}\right) + c.c. \quad (24)$$

As in the three-dimensional case, we find that the carrier frequency is $\omega_0/(1-M^2)$, and that refocusing is enhanced when the source is moving, both in the direction of the source motion and in the transverse directions, with the enhancement factor $1/(1-M^2)$ in the longitudinal direction and $1/\sqrt{1-M^2}$ in the transverse one (see [Fig. 5](#)).

In the supersonic regime $M > 1$, if the bandwidth of f is smaller than ω_0 , then we find

$$u_{\text{tr}}(t, \vec{\mathbf{x}}) = \frac{-\text{sgn}(z - Z_0 + Mc_0 t)}{4\sqrt{M^2 - 1}} \exp\left(i\omega_0 \frac{t + M \frac{z-Z_0}{c_0}}{M^2 - 1}\right) f\left(\frac{t + M \frac{z-Z_0}{c_0}}{M^2 - 1}\right) \mathcal{J}\left(\frac{\omega_0}{c_0} \frac{|z - Z_0 + Mc_0 t|}{M^2 - 1}, \frac{\omega_0}{c_0} \frac{|x - X_0|}{\sqrt{M^2 - 1}}\right) + c.c., \quad (25)$$

where

$$\mathcal{J}(a, b) = \begin{cases} 0, & \text{if } b > a, \\ J_0(\sqrt{a^2 - b^2}), & \text{if } a > b. \end{cases} \quad (26)$$

Note that the carrier frequency is $\omega_0/(M^2 - 1)$ and that inside the Mach cone the refocused wave oscillates and decays slowly as a square root (this is the behavior of J_0). The Mach cone is defined by the usual formula $|z - Z_0 + vt| = \sqrt{M^2 - 1}|x - X_0|$ (see [Fig. 6](#)).

Remark. The expressions of the refocused time-reversed wave for a subsonic or a supersonic source with arbitrary bandwidth are given in [Appendix C](#). The resolution properties are qualitatively as discussed above.

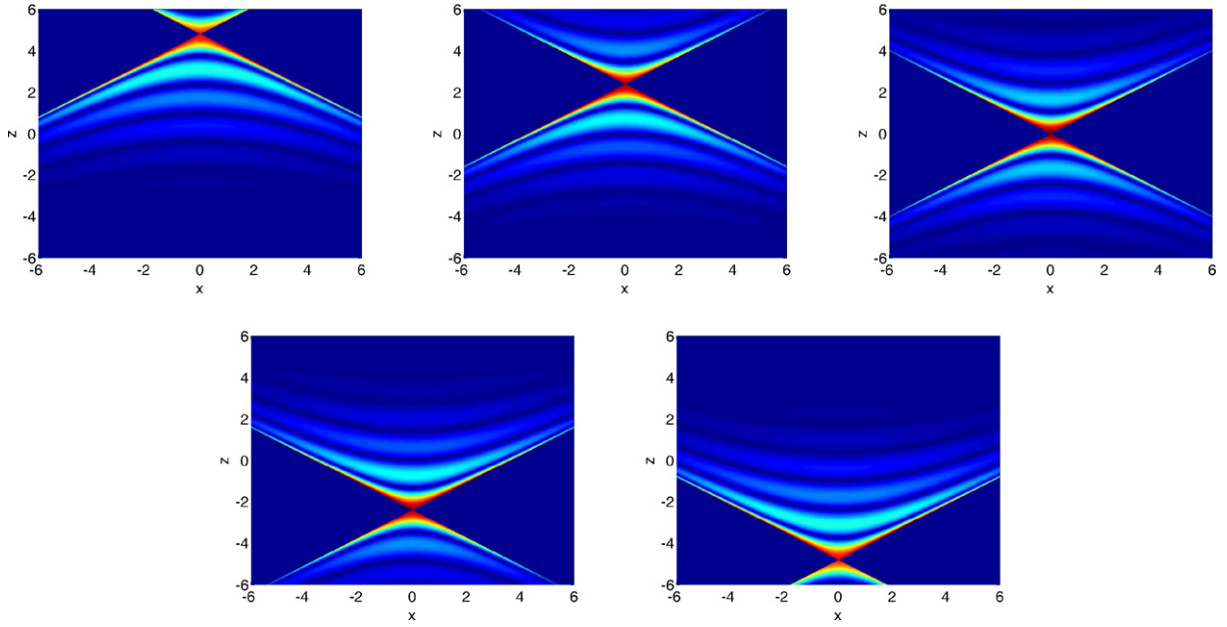


Fig. 6. Spatial profile of the time-reversed refocused wave at $t = -4, -2, 0, 2, 4$ with Neumann data when $M = v/c_0 = 1.2$, $\omega_0 = 1$, $c_0 = 1$, and the source pulse is $f(t) = \exp(-B^2t^2)$, $B = 0.1$. The set-up is two-dimensional.

4.2. Two-dimensional time reversal with a partial-aperture mirror

We revisit the analysis of the time-reversal experiment in a two-dimensional set-up, for a moving source and for a time-reversal mirror that covers the line $[-a/2, a/2] \times \{0\}$. As we will see, the results for time-reversal refocusing are similar as those in the three-dimensional set-up.

We consider a moving point-like source emitting a signal with carrier frequency ω_0 and pulse profile $f(t)$. The source position is

$$\vec{\mathbf{X}}(t) = \vec{\mathbf{X}}_0 + \vec{\mathbf{V}}_0 t,$$

where $\vec{\mathbf{X}}_0 = (X_0, Z_0)$ and $\vec{\mathbf{V}}_0 = (V_x, V_z)$. We consider the paraxial regime in which $|X_0| \ll Z_0$ and $\lambda_0 \ll a \ll Z_0$. We also assume that the bandwidth B of the source is smaller than the carrier frequency ω_0 . Therefore the normal derivative of the field recorded at the time-reversal mirror is

$$\partial_\nu \hat{u}(\omega, \vec{\mathbf{x}}) = \frac{\sqrt{\omega} e^{-i\frac{\pi}{4}}}{2\sqrt{2\pi c_0 Z_0}} \exp\left(i\frac{\omega}{c_0} \left(Z_0 + \frac{(x - X_0)^2}{2Z_0}\right)\right) \hat{f}\left(\omega \left(1 + \frac{V_z}{c_0} + \frac{V_x(X_0 - x)}{c_0 Z_0}\right) - \omega_0\right) + s.c.,$$

for $\vec{\mathbf{x}} = (x, 0)$, $x \in [-a/2, a/2]$. Here we have used the asymptotic form of the Hankel function $H_0^{(1)}(q) \simeq \sqrt{2/(\pi q)} \exp(iq - i\pi/4)$ for $q \gg 1$. The time-reversed wave field for $\vec{\mathbf{x}} = \vec{\mathbf{X}}_0 + (\xi, \eta)$ with $|\eta| \ll Z_0$ and $\frac{\omega_0}{c_0} \xi^2 \ll Z_0$ is

$$u_{tr}(t, \vec{\mathbf{x}}) = \frac{i}{8\pi Z_0} \int_{-a/2}^{a/2} \exp\left(i\frac{\omega_0}{c_0} \frac{-c_0 t + \eta + \frac{\xi(X_0 - x')}{Z_0} - \frac{\eta(X_0 - x')^2}{2Z_0^2}}{1 + \frac{V_z}{c_0} + \frac{V_x(X_0 - x')}{c_0 Z_0}}\right) \times \frac{1}{\left|1 + \frac{V_z}{c_0} + \frac{V_x(X_0 - x')}{c_0 Z_0}\right|} f\left(\frac{-c_0 t + \eta + \frac{\xi(X_0 - x')}{Z_0} - \frac{\eta(X_0 - x')^2}{2Z_0^2}}{c_0 \left(1 + \frac{V_z}{c_0} + \frac{V_x(X_0 - x')}{c_0 Z_0}\right)}\right) dx' + c.c. \tag{27}$$

This expression can be simplified as explained below.

Main results. If $a^2/Z_0^2 \ll B/\omega_0 \ll 1$, then the time-reversed wave field is of the form

$$u_{tr}(t, \vec{\mathbf{x}}) = \frac{ia}{8\pi Z_0 |1 + M_\nu|} \text{sinc}\left(\frac{\omega_0 a}{2c_0 Z_0 (1 + M_\nu)^2} \left(\left(\xi - \eta \frac{X_0}{Z_0}\right) \left(1 + \frac{V_z}{c_0}\right) - \frac{V_x}{c_0} (\eta - c_0 t)\right)\right) \times \exp\left(i\frac{\omega_0}{c_0 (1 + M_\nu)} \left(\eta \left(1 - \frac{X_0^2}{2Z_0^2}\right) + \xi \frac{X_0}{Z_0} - c_0 t\right)\right) f\left(\frac{\eta \left(1 - \frac{X_0^2}{2Z_0^2}\right) + \xi \frac{X_0}{Z_0} - c_0 t}{c_0 (1 + M_\nu)}\right) + c.c., \tag{28}$$

where we have introduced the parameter

$$M_v = \frac{V_z}{c_0} + \frac{V_x X_0}{c_0 Z_0} = \frac{\vec{V}_0 \cdot \vec{X}_0}{c_0 Z_0}. \quad (29)$$

The Doppler effect is responsible for a shift in the carrier frequency of the recorded data that becomes $\omega_0/|1 + M_v|$. As a result the cross-range resolution is the standard Rayleigh resolution formula $\lambda_{\text{eff}} Z_0/a$, with $\lambda_{\text{eff}} = \lambda_0|1 + M_v|$. The range resolution is c_0/B_{eff} , with $B_{\text{eff}} = B/|1 + M_v|$.

If $B/\omega_0 \ll a^2/Z_0^2 \ll 1$ (quasi-monochromatic case), then

$$u_{\text{tr}}(t, \vec{x}) = \frac{ia}{8\pi Z_0|1 + M_v|} \exp\left(i \frac{\omega_0}{c_0(1 + M_v)} \left(\eta \left(1 - \frac{X_0^2}{2Z_0^2}\right) + \xi \frac{X_0}{Z_0} - c_0 t\right)\right) f(0) \\ \times \Psi\left(\frac{\omega_0 a}{c_0 Z_0(1 + M_v)^2} \left(\left(\xi - \eta \frac{X_0}{Z_0}\right) \left(1 + \frac{V_z}{c_0}\right) - \frac{V_x}{c_0} (\eta - c_0 t)\right), \frac{\omega_0 a^2}{2c_0 Z_0^2(1 + M_v)} \eta\right) + c.c., \quad (30)$$

where Ψ is defined by (22). Here the cross-range resolution is $\lambda_{\text{eff}} Z_0/a$ but the range resolution is $\lambda_{\text{eff}} Z_0^2/a^2$, with $\lambda_{\text{eff}} = \lambda_0|1 + M_v|$.

5. Conclusions

This paper analyzes time-reversal refocusing for a moving source and shows resolution enhancement when the source velocity becomes non-negligible compared to the wave speed. This phenomenon is essentially independent of the dimension and it can be related to Doppler effects that allow the time-reversal mirror to record information with a bandwidth that is larger than the source bandwidth.

If the source is subsonic then the time-reversed refocused spot has the same form as in the case of a stationary source, but in a stretched space. The formulas are especially simple in the full-aperture case (when the time-reversal mirror surrounds the original source), as we recover the classical diffraction-limited focal spots, but with a stretching by a factor $1 - M^2$ in the longitudinal direction (along the velocity vector) and $\sqrt{1 - M^2}$ in the transverse direction(s) (M is the Mach number). When the mirror has partial aperture, the enhancement factors depend on the norm and direction of the velocity vector. If the velocity vector of the source is pointed towards the time-reversal array, then resolution is enhanced compared to the case of a stationary source. If the velocity vector is pointed away from the time-reversal array, then resolution is reduced.

Similar results have been presented for a supersonic source. The refocused spatial spot for a full-aperture mirror exhibits a nearly-infinite resolution as the original source location is at the interaction of two Mach cones.

Acknowledgments

This work was supported by LABEX WIFI (Laboratory of Excellence ANR-10-LABX-24) within the French Program Investments for the Future under reference ANR-10-IDEX-0001-02 PSL*, by ANR project SURMITO, and by ERC Advanced Grant Project MULTIMOD-267184.

Appendix A. Proof of (6) and (8)

We consider the expression (5) of the refocused wave in the subsonic case $M < 1$, which can be written as

$$u_{\text{tr}}(t, \vec{x}) = \frac{1}{16\pi^2 c_0} \int_{-\infty}^{\infty} d\omega (-i\omega) \overline{\hat{f}(\omega - \omega_0)} I\left(\omega t, \frac{|\omega|}{c_0} |\mathbf{x} - \mathbf{X}_0|, \frac{\omega}{c_0} (z - Z_0)\right) + c.c., \quad (A.1)$$

with

$$I(\tilde{t}, \tilde{x}, \tilde{z}) = \int_{-1}^1 \frac{1}{(1 - Mq)^2} J_0\left(\frac{\sqrt{1 - q^2}}{1 - Mq} \tilde{x}\right) e^{-i \frac{\tilde{t} + \tilde{z}q}{1 - Mq}} dq.$$

By the change of variable $r = \frac{1 - M^2}{2M} \left(\frac{1}{1 - Mq} - \frac{1}{1 + M}\right)$, we get

$$I(\tilde{t}, \tilde{x}, \tilde{z}) = \frac{2}{1 - M^2} \int_0^1 J_0\left(\frac{2\tilde{x}}{1 - M^2} \sqrt{r - r^2}\right) e^{-2i \frac{M\tilde{t} + \tilde{z}}{1 - M^2} r - i \frac{\tilde{t} - \tilde{z}}{1 + M}} dr.$$

Then we apply the change of variable $r = \cos^2(\theta/2)$:

$$I(\tilde{t}, \tilde{x}, \tilde{z}) = \frac{1}{1 - M^2} \int_0^\pi J_0\left(\frac{\tilde{x}}{1 - M^2} \sin \theta\right) \exp\left(i \frac{M\tilde{t} + \tilde{z}}{1 - M^2} \cos \theta\right) \sin \theta d\theta \exp\left(-i \frac{\tilde{t} + M\tilde{z}}{1 - M^2}\right) \\ = \frac{2}{1 - M^2} \int_0^{\pi/2} J_0\left(\frac{\tilde{x}}{1 - M^2} \sin \theta\right) \cos\left(\frac{M\tilde{t} + \tilde{z}}{1 - M^2} \cos \theta\right) \sin \theta d\theta \exp\left(-i \frac{\tilde{t} + M\tilde{z}}{1 - M^2}\right),$$

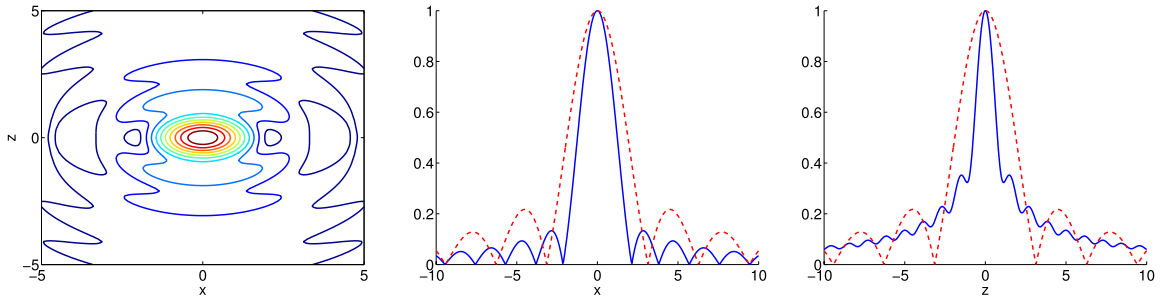


Fig. B.1. Spatial profile of the time-reversed refocused wave at $t = 0$ with Dirichlet data when $M = v/c_0 = 0.8$. In the center and right figures, the dashed red lines are the standard sinc function when the source does not move. (For interpretation of the references to color in this figure legend, the reader is referred to the web version of this article.)

and we use [33, formula 6.688.2] which gives:

$$I(\tilde{t}, \tilde{x}, \tilde{z}) = \frac{2}{1 - M^2} \operatorname{sinc} \left(\sqrt{\frac{\tilde{x}^2}{1 - M^2} + \frac{(\tilde{z} + M\tilde{t})^2}{(1 - M^2)^2}} \right) \exp \left(-i \frac{\tilde{t} + M\tilde{z}}{1 - M^2} \right). \tag{A.2}$$

Substituting into (A.1) we find the expression of the time-reversed wave valid for arbitrary bandwidth. If the bandwidth of \hat{f} is small, then we get (6).

The derivation of (8) from (7) when $M > 1$ follows the same line and makes use of [33, formula 6.737.5] (instead of [33, formula 6.688.2] as above), so we get

$$\int_{-1}^1 \frac{\operatorname{sgn}(1 - Mq)}{(1 - Mq)^2} J_0 \left(\frac{\sqrt{1 - q^2}}{|1 - Mq|} \tilde{x} \right) e^{-i \frac{\tilde{t} + \tilde{z}q}{1 - Mq}} dq = \frac{2i \operatorname{sgn}(\tilde{z} + M\tilde{t})}{M^2 - 1} \Phi \left(\frac{|\tilde{z} + M\tilde{t}|}{M^2 - 1}, \frac{\tilde{x}}{\sqrt{M^2 - 1}} \right) \exp \left(i \frac{\tilde{t} + M\tilde{z}}{M^2 - 1} \right), \tag{A.3}$$

with Φ defined by (9).

Appendix B. Dirichlet data

Throughout the paper we have addressed time reversal using Neumann data. For the sake of completeness, we briefly address the case of Dirichlet data to show that the results are not qualitatively affected. We consider the same set-up as in Section 2, but the mirror records the field itself and not its normal derivative, so that the Dirichlet data set is (in the frequency domain):

$$\{ \hat{u}(\omega, \vec{x}) + c.c., \vec{x} \in \partial B(\mathbf{0}, L) \}, \tag{B.1}$$

instead of (3). The time-reversal mirror re-emits the time-reversed recorded signals so that the time-reversed wave field is

$$\hat{u}_{\text{dir}}(\omega, \vec{x}) = \int_{\partial B(\mathbf{0}, L)} \hat{G}(\omega, \vec{x}, \vec{x}') \overline{\hat{u}(\omega, \vec{x}')} d\sigma(\vec{x}') + s.c. \tag{B.2}$$

If the search point \vec{x} is close to the center $\mathbf{0}$, that is to say, $|\vec{x}| \ll L$ and $\frac{\omega_0}{c_0} |\vec{x}|^2 \ll L$, then the time-reversed wave field is

$$u_{\text{dir}}(t, \vec{x}) = \frac{1}{8\pi} \int_{-1}^1 \frac{1}{|1 - Mq|} J_0 \left(\frac{\sqrt{1 - q^2}}{|1 - Mq|} \frac{\omega_0 |\mathbf{x} - \mathbf{X}_0|}{c_0} \right) \times \exp \left(-i\omega_0 \frac{t + \frac{z - Z_0}{c_0} q}{1 - Mq} \right) f \left(-\frac{t + \frac{z - Z_0}{c_0} q}{1 - Mq} \right) dq + c.c.,$$

provided the bandwidth (of f) is smaller than the carrier frequency ω_0 . The modulus of this function is plotted in Fig. B.1 at time 0 for $f \equiv 1$. By comparing with Fig. 1 one can see that the peak has the same width, but the lobes (in the longitudinal direction) are larger with Dirichlet data than with Neumann data.

Appendix C. Proof of (24) and (25)

We consider the expression (23) of the refocused wave which can be written as

$$\hat{u}_{\text{tr}}(\omega, \vec{x}) = \frac{-i}{8\pi v} \int_{-\infty}^{\infty} \int_{\mathbb{R}} J_0 \left(\frac{\omega}{c_0} \sqrt{(x - X_0)^2 + \zeta^2} \right) e^{i \frac{\omega' - \omega}{v} \zeta} d\zeta e^{i \frac{\omega' - \omega}{v} (z - Z_0)} \overline{\hat{f}(\omega' - \omega_0)} d\omega'.$$

In this appendix we do write the c.c. and s.c. terms. Using formula [33, formula 6.677.3] to compute the integral with respect to ζ , we get

$$\begin{aligned} \hat{u}_{\text{tr}}(\omega, \vec{\mathbf{x}}) &= \frac{-i}{4\pi} \operatorname{sgn}(\omega) \int_{-\infty}^{\infty} \frac{\cos\left(\frac{|x-X_0|}{Mc_0} \sqrt{M^2\omega^2 - (\omega' - \omega)^2}\right)}{\sqrt{M^2\omega^2 - (\omega' - \omega)^2}} \\ &\quad \times e^{i\frac{\omega' - \omega}{Mc_0}(z-Z_0)} \mathbf{1}_{M|\omega| > |\omega' - \omega|} \overline{\hat{f}(\omega' - \omega_0)} d\omega'. \end{aligned} \quad (\text{C.1})$$

In the subsonic regime $M \in (0, 1)$, this can be written as

$$\begin{aligned} \hat{u}_{\text{tr}}(\omega, \vec{\mathbf{x}}) &= \frac{-i}{4\pi} \operatorname{sgn}(\omega) \int_{-\infty}^{\infty} \frac{\cos\left(\frac{|x-X_0|\sqrt{1-M^2}}{c_0M} \sqrt{\left(\omega - \frac{\omega'}{1+M}\right)\left(\frac{\omega'}{1-M} - \omega\right)}\right)}{\sqrt{1-M^2} \sqrt{\left(\omega - \frac{\omega'}{1+M}\right)\left(\frac{\omega'}{1-M} - \omega\right)}} \\ &\quad \times e^{i\frac{\omega' - \omega}{Mc_0}(z-Z_0)} \mathbf{1}_{\frac{\omega'}{1+M\operatorname{sgn}(\omega)} < \omega < \frac{\omega'}{1-M\operatorname{sgn}(\omega)}} \overline{\hat{f}(\omega' - \omega_0)} d\omega'. \end{aligned}$$

In the time domain

$$\begin{aligned} u_{\text{tr}}(t, \vec{\mathbf{x}}) &= \frac{1}{2\pi} \int_{-\infty}^{\infty} \hat{u}_{\text{tr}}(\omega, \vec{\mathbf{x}}) e^{-i\omega t} d\omega \\ &= \frac{-i}{8\pi^2} \int_{-\infty}^{\infty} \int_{-\frac{M|\omega'|}{1-M^2}}^{\frac{M|\omega'|}{1-M^2}} \frac{\cos\left(\frac{|x-X_0|\sqrt{1-M^2}}{c_0M} \sqrt{\frac{\omega'^2 M^2}{(1-M^2)^2} - \omega^2}\right)}{\sqrt{1-M^2} \sqrt{\frac{\omega'^2 M^2}{(1-M^2)^2} - \omega^2}} \\ &\quad \times \exp\left(-i\omega\left(t + \frac{z-Z_0}{Mc_0}\right)\right) d\omega \operatorname{sgn}(\omega') e^{-i\frac{\omega'}{1-M^2}\left(t+M\frac{z-Z_0}{c_0}\right)} \overline{\hat{f}(\omega' - \omega_0)} d\omega' \\ &= \frac{-i}{4\pi^2 \sqrt{1-M^2}} \int_{-\infty}^{\infty} \int_0^1 \frac{\cos\left(\frac{\omega'|x-X_0|}{c_0\sqrt{1-M^2}} \sqrt{1-q^2}\right)}{\sqrt{1-q^2}} \\ &\quad \times \cos\left(\frac{\omega'}{1-M^2}\left(Mt + \frac{z-Z_0}{c_0}\right)q\right) dq \operatorname{sgn}(\omega') e^{-i\frac{\omega'}{1-M^2}\left(t+M\frac{z-Z_0}{c_0}\right)} \overline{\hat{f}(\omega' - \omega_0)} d\omega'. \end{aligned}$$

After the change of variable $q = \sin \phi$ and the use of the formula $\int_0^\pi e^{ix \sin \phi} d\phi = \pi J_0(x)$ [33, formula 8.411.1] which implies

$$\int_0^{\pi/2} \cos(a \cos \phi) \cos(b \cos \phi) d\phi = \frac{\pi}{2} J_0(\sqrt{a^2 + b^2}),$$

we get

$$\begin{aligned} u_{\text{tr}}(t, \vec{\mathbf{x}}) &= \frac{-i}{8\pi \sqrt{1-M^2}} \int_{-\infty}^{\infty} J_0\left(\frac{|\omega'|}{c_0} \sqrt{\frac{|x-X_0|^2}{1-M^2} + \frac{(z-Z_0 + Mc_0 t)^2}{(1-M^2)^2}}\right) \\ &\quad \times \operatorname{sgn}(\omega') e^{-i\frac{\omega'}{1-M^2}\left(t+M\frac{z-Z_0}{c_0}\right)} \overline{\hat{f}(\omega' - \omega_0)} d\omega'. \end{aligned} \quad (\text{C.2})$$

This formula is valid whatever the bandwidth of f . If the bandwidth is smaller than ω_0 , then we get (24).

In the supersonic regime $M > 1$, Eq. (C.1) can be written as

$$\begin{aligned} \hat{u}_{\text{tr}}(\omega, \vec{\mathbf{x}}) &= \frac{-i}{4\pi} \int_{-\infty}^{\infty} \frac{\cos\left(\frac{|x-X_0|\sqrt{M^2-1}}{Mc_0} \sqrt{\left(\omega - \frac{\omega'}{M+1}\right)\left(\frac{\omega'}{M-1} + \omega\right)}\right)}{\sqrt{M^2-1} \sqrt{\left(\omega - \frac{\omega'}{M+1}\right)\left(\frac{\omega'}{M-1} + \omega\right)}} e^{i\frac{\omega' - \omega}{c_0M}(z-Z_0)} \\ &\quad \times \left(\mathbf{1}_{\omega > \max\left(\frac{\omega'}{M+1}, -\frac{\omega'}{M-1}\right)} - \mathbf{1}_{\omega < \min\left(\frac{\omega'}{M+1}, -\frac{\omega'}{M-1}\right)}\right) \overline{\hat{f}(\omega' - \omega_0)} d\omega'. \end{aligned}$$

In the time domain

$$u_{\text{tr}}(t, \vec{\mathbf{x}}) = \frac{1}{2\pi} \int_{-\infty}^{\infty} \hat{u}_{\text{tr}}(\omega, \vec{\mathbf{x}}) e^{-i\omega t} d\omega$$

$$\begin{aligned}
 &= \frac{-i}{8\pi^2} \int_{-\infty}^{\infty} \int_{-\infty}^{\infty} \frac{\cos\left(\frac{|x-X_0|\sqrt{M^2-1}}{c_0 M} \sqrt{\frac{\omega^2-\omega'^2 M^2}{(M^2-1)^2}}\right)}{\sqrt{M^2-1} \sqrt{\omega^2 - \frac{\omega'^2 M^2}{(M^2-1)^2}}} \exp\left(-i\omega\left(t + \frac{z-Z_0}{Mc_0}\right)\right) \\
 &\quad \times \left(\mathbf{1}_{\omega > \frac{|\omega'|}{M^2-1}} - \mathbf{1}_{\omega < -\frac{|\omega'|}{M^2-1}}\right) d\omega e^{i\frac{\omega'}{M^2-1}\left(t+M\frac{z-Z_0}{c_0}\right)} \widehat{f}(\omega' - \omega_0) d\omega' \\
 &= \frac{-1}{4\pi^2 \sqrt{M^2-1}} \int_{-\infty}^{\infty} \int_1^{\infty} \frac{\cos\left(\frac{\omega'|x-X_0|}{c_0 \sqrt{M^2-1}} \sqrt{q-1}\right)}{\sqrt{q-1}} \\
 &\quad \times \sin\left(\frac{|\omega'|}{M^2-1}\left(Mt + \frac{z-Z_0}{c_0}\right)q\right) dq e^{i\frac{\omega'}{M^2-1}\left(t+M\frac{z-Z_0}{c_0}\right)} \widehat{f}(\omega' - \omega_0) d\omega'.
 \end{aligned}$$

After the change of variable $q = \cosh \phi$ and the use of the formula $\int_0^\infty \sin(x \cosh \phi) d\phi = \pi J_0(x)/2$ [33, formula 8.411.11] which implies

$$\int_0^\infty \sin(a \cosh \phi) \cos(b \sinh \phi) d\phi = \begin{cases} 0 & \text{if } b > a > 0, \\ \frac{\pi}{2} J_0(\sqrt{a^2 - b^2}) & \text{if } a > b > 0, \end{cases}$$

we get

$$\begin{aligned}
 u_{\text{tr}}(t, \vec{x}) &= \frac{-1}{8\pi \sqrt{M^2-1}} \operatorname{sgn}\left(Mt + \frac{z-Z_0}{c_0}\right) \int_{-\infty}^{\infty} \mathcal{J}\left(\frac{|\omega'|}{c_0} \frac{|z-Z_0 + Mc_0 t|}{M^2-1}, \frac{|\omega'|}{c_0} \frac{|x-X_0|}{\sqrt{M^2-1}}\right) \\
 &\quad \times e^{i\frac{\omega'}{M^2-1}\left(t+M\frac{z-Z_0}{c_0}\right)} \widehat{f}(\omega' - \omega_0) d\omega'.
 \end{aligned} \tag{C.3}$$

This formula is valid whatever the bandwidth of f . If the bandwidth is smaller than ω_0 , then we get (25).

References

- [1] M. Fink, Time reversal of ultrasonic fields. I. Basic principles, IEEE Trans. Ultrason. Ferroelectr. Freq. Control 39 (1992) 555–566.
- [2] M. Fink, Time reversed acoustics, Sci. Am. 281 (1999) 91–97.
- [3] M. Fink, D. Cassereau, A. Derode, C. Prada, P. Roux, M. Tanter, J.-L. Thomas, F. Wu, Time-reversed acoustics, Rep. Progr. Phys. 63 (2000) 1933–1995.
- [4] L. Borcea, G. Papanicolaou, C. Tsogka, J. Berryman, Imaging and time reversal in random media, Inverse Problems 18 (2002) 1247–1279.
- [5] J. de Rosny, G. Lerosee, M. Fink, Theory of electromagnetic time-reversal mirrors, IEEE Trans. Antennas and Propagation 58 (2010) 3139–3149.
- [6] J. de Rosny, A. Tourin, A. Derode, P. Roux, M. Fink, Weak localization and time reversal of ultrasound in a rotational flow, Phys. Rev. Lett. 95 (2005) 074301.
- [7] D. Cassereau, M. Fink, Time reversal of ultrasonic fields—part III: theory of the closed time-reversal cavity, IEEE Trans. Ultrason. Ferroelectr. Freq. Control 39 (1992) 579–592.
- [8] W. Elmore, M. Heald, Physics of Waves, Dover, New York, 1969.
- [9] S. Kim, G.F. Edelmann, W.S. Hodgkiss, W.A. Kuperman, H.C. Song, T. Akal, Spatial resolution of time-reversal arrays in shallow water, J. Acoust. Soc. Am. 110 (2001) 820–829.
- [10] J. de Rosny, M. Fink, Overcoming the diffraction limit in wave physics using a time-reversal mirror and a novel acoustic sink, Phys. Rev. Lett. 89 (2002) 124301.
- [11] J. de Rosny, M. Fink, Focusing properties of near-field time reversal, Phys. Rev. A 76 (2007) 065801.
- [12] G. Lerosee, J. de Rosny, A. Tourin, M. Fink, Focusing beyond the diffraction limit with far-field time reversal, Science 315 (2007) 1120–1122.
- [13] P. Blomgren, G. Papanicolaou, H. Zhao, Super-resolution in time-reversal acoustics, J. Acoust. Soc. Am. 111 (2002) 230–248.
- [14] A. Derode, P. Roux, M. Fink, Robust acoustic time reversal with high order multiple scattering, Phys. Rev. Lett. 75 (1995) 4206–4209.
- [15] A. Derode, A. Tourin, J. de Rosny, M. Tanter, S. Yon, M. Fink, Taking advantage of multiple scattering to communicate with time-reversal antennas, Phys. Rev. Lett. 90 (2003) 014301.
- [16] J. de Rosny, A. Tourin, A. Derode, B. van Tiggelen, M. Fink, Relation between time reversal focusing and coherent backscattering in multiple scattering media: a diagrammatic approach, Phys. Rev. E 70 (2004) 046601.
- [17] J.-P. Fouque, J. Garnier, A. Nachbin, K. Sølna, Time reversal refocusing for point source in randomly layered media, Wave Motion 42 (2005) 238–260.
- [18] J.-P. Fouque, J. Garnier, K. Sølna, Time reversal super resolution in randomly layered media, Wave Motion 43 (2006) 646–666.
- [19] J.-P. Fouque, J. Garnier, G. Papanicolaou, K. Sølna, Wave Propagation and Time Reversal in Randomly Layered Media, Springer, New York, 2007.
- [20] J. Garnier, G. Papanicolaou, Pulse propagation and time reversal in random waveguides, SIAM J. Appl. Math. 67 (2007) 1718–1739.
- [21] A. Tourin, M. Fink, A. Derode, Multiple scattering of sound, Waves Random Media 10 (2000) R31–R60.
- [22] D.R. Dowling, D.R. Jackson, Narrow-band performance of phase-conjugate arrays in dynamic random media, J. Acoust. Soc. Am. 91 (1992) 3257–3277.
- [23] M. Dungan, D.R. Dowling, Computed narrow-band time-reversing array retrofocusing in a dynamic shallow ocean, J. Acoust. Soc. Am. 107 (2000) 3101–3112.
- [24] D.G. Alfaro Vigo, J.-P. Fouque, J. Garnier, A. Nachbin, Robustness of time reversal for waves in time-dependent random media, Stochastic Process. Appl. 111 (2004) 289–313.
- [25] K.G. Sabra, D.R. Dowling, Broadband performance of a moving time reversing array, J. Acoust. Soc. Am. 114 (2003) 1395–1405.
- [26] K.G. Sabra, D.R. Dowling, Broadband performance of a time reversing array with a moving source, J. Acoust. Soc. Am. 115 (2004) 2807–2817.
- [27] T. Shimura, H. Ochi, Y. Watanabe, Time-reversal communication with moving source-receiver in shallow water, Japan. J. Appl. Phys. 45 (2006) 4847–4852.
- [28] H.C. Song, W.S. Hodgkiss, W.A. Kuperman, W.J. Higley, K. Raghukumar, T. Akal, M. Stevenson, Spatial diversity in passive time reversal communications, J. Acoust. Soc. Am. 120 (2006) 2067–2076.
- [29] H.C. Song, Time reversal communication with a mobile source, J. Acoust. Soc. Am. 134 (2013) 2623–2626.
- [30] F.D. Philippe, C. Prada, M. Fink, J. Garnier, J. de Rosny, Analysis of the time reversal operator for a scatterer undergoing small displacements, J. Acoust. Soc. Am. 133 (2013) 94–107.
- [31] M. Born, E. Wolf, Principles of Optics, Cambridge University Press, Cambridge, 1999.
- [32] H. Ammari, J. Garnier, W. Jing, H. Kang, M. Lim, K. Sølna, H. Wang, Mathematical and Statistical Methods for Multistatic Imaging, in: Lecture Notes in Mathematics, vol. 2098, Springer, Berlin, 2013.
- [33] I.S. Gradshteyn, I.M. Ryzhik, Tables of Integrals, Sums, Series, and Products, Academic Press, New York, 1980.
- [34] U. Vilaipornsawai, A.J. Silva, S.M. Jesus, Underwater communications for moving source using geometry-adapted time reversal and DFE: UAN10 data, in: OCEANS 2011 IEEE Conference, Santandar, Spain, June 2011, pp. 1–7.